

Tuning electronic properties in transition metal dichalcogenides MX_2 (M= Mo/W, X= S/Se) heterobilayers with strain and twist angle

Ravina Beniwal^a, M. Suman Kalyan^b, Nicolas Leconte^c, Jeil

Jung^{c,d,*}, Bala Murali Krishna Mariserla^{a,*}, S. Appalakondaiah^{a,e,*}

^aDepartment of Physics, Indian Institute of Technology Jodhpur, Rajasthan, India-342037*

^bDepartment of Physics, National Institute of Technology Agartala, Agartala - 799046, Tripura, India.

^cDepartment of Physics, University of Seoul, Seoul 02504, Korea

^dDepartment of Smart Cities, University of Seoul, Seoul 02504, Korea[†] and

^eDepartment of Physics, Pondicherry University, Kalapet, Puducherry 605 014, India

(Dated: December 12, 2023)

We explore the direct to indirect band gap transitions in MX_2 (M= Mo/W, X= S/Se) transition metal dichalcogenides heterobilayers for different system compositions, strains, and twist angles based on first principles density functional theory calculations within the G_0W_0 approximation. The obtained band gaps that typically range between 1.4–2.0 eV are direct/indirect for different/same chalcogen atom systems and can often be induced through expansive/compressive biaxial strains of a few percent. A direct to indirect gap transition is verified for heterobilayers upon application of a finite 16° twist that weakens interlayer coupling. The large inter-layer exciton binding energies of the order of ~ 250 meV estimated by solving the Bethe-Salpeter equation suggest these systems are amenable to be studied through infrared and Raman spectroscopy.

I. INTRODUCTION

Among the wide range of 2-dimensional (2D) materials, transition metal dichalcogenides (TMD) are promising due to their valley-dependent electronic structure [1, 2], strong excitonic (electron-hole pair) effects [3–5], and enhanced photoluminescence (PL) that make these ultra-thin materials suitable for novel flexible optoelectronic devices [6, 7]. The artificial stacking of 2D layers as homo/hetero-bilayers allows to tune the optoelectronic properties resulting in proposals of broadband photodetectors and flexible atomically thin p-n junction transistors [8–11]. When van der Waals (vdW) homo/heterobilayers are composed of semiconductors, they have staggered band alignment which facilitates interlayer excitons due to charge transfer across the interfaces [12–16]. The exciton charges are spatially separated in different layers of TMD heterobilayers and hence endow them with long lifetimes lasting from hundreds of nano to micro seconds [17, 18]. The spatial charge separation between electron-hole pairs induces a permanent dipole moment, allowing electrically controlled optical and transport properties [19]. These are systems with binding energies greater than 100 meV, making them suitable for developing devices that operate at room-temperature [20].

Generally, the binding energies are lower for interlayer excitons in contrast to intralayer excitons. Particularly, monolayer TMD such as MX_2 (M= Mo, W, and X = S, Se), have exceptionally high exciton binding energies (320-700 meV) [3, 4, 21], while these energies are reduced in bilayers [80-450 meV] due to dielectric screen-

ing [21–23]. Previous studies on the same chalcogen-centric heterobilayers MoS_2/WS_2 and $\text{MoSe}_2/\text{WSe}_2$ having very small lattice mismatch (0.3%) displayed their indirect band gap behavior in the near-IR region with interlayer exciton binding energies of 250-450 meV respectively [13, 24]. The experimental studies based on TMD monolayers throw some light on dark excitons, which can interact with bright excitons and allow them to carry energy and information [25–27]. The investigation of valley-polarized dark excitons in $\text{MoSe}_2/\text{WSe}_2$ reveals microsecond lifetimes, making them promising candidates for valleytronic devices and quantum computers [18].

Currently, most of the theoretical studies on TMD heterobilayers are focused on electronic, optical, and vibrational properties of same chalcogen atom monolayers or bilayers [28–31]. However, there are limited reports on the electronic properties of different chalcogen atom heterobilayers [32–34]. Since lattice mismatch is arising in the heterobilayers, the band offset and band gap nature plays a crucial role in defining the optoelectronic properties, which remain yet to be examined. In this work, we have explored the ground-state electronic properties of same and different chalcogen-based heterobilayers and studied the nature of the band gaps as function of strain and twist angle. In our calculations, we carried out a systematic investigation of the vibrational properties, electronic band gap, and intra/interlayer exciton behavior using first-principles calculations for MX_2 (M= Mo/W, X= S/Se) heterobilayers. We explore the effects of strains and twist angles which clearly show the influence of interlayer interactions and lattice mismatch on aforementioned materials.

This paper is structured as follows: Section II describes the computational methodologies used to study the heterobilayers. In section III A, we present structural and vibrational properties of TMD heterobilayers, followed by electronic properties in section III B and the absorp-

* bmkrishna@iitj.ac.in; kondaiah@pondiuni.ac.in

[†] jeiljung@uos.ac.kr

tion spectra in section III C. Band gap tuning of these structures through mechanical strain and twist angle is shown in Section III D. We conclude the paper by summarizing our results in section IV.

II. COMPUTATIONAL DETAILS

The ground state and lattice dynamic calculations have been performed using plane-wave pseudopotential method implemented in Quantum Espresso [35]. We have used LDA-CAPZ [36] approximation as an exchange-correlation function and the vdW interactions are captured with the opt-vdW86B dispersion correction [37]. We considered 120 Ry plane wave kinetic energy cutoff with $16 \times 16 \times 1$ k-point grid in the Brillouin zone and added a vacuum height of 12 Å to relax all heterobilayers. The Kohn–Sham self-consistent total energy was converged within 1E-8 eV. For both lattice and atomic relaxations, the positions of the atoms were allowed to relax until the forces were less than 1E-4 eV/Å. To compute the Raman frequencies, we applied DFPT method with norm-conserving pseudopotentials [38]. It is well-known that the Kohn-Sham calculations in DFT usually result in a bandstructure with underestimated band gaps. We have thus used the G_0W_0 approximation given by Vienna Ab-initio Simulation Package (VASP) to get a quasi-particle electronic bandstructure [39]. To achieve convergence, we utilized 432 bands for the summation over bands in the polarizability and self-energy calculations. Polarizability matrices are calculated up to a cutoff of 400 eV. We have studied excitonic properties by solving Bethe-Salpeter equation (BSE) [40]. We considered the highest occupied valence and lowest unoccupied conduction bands as 18 and 22, respectively. The tunability of bandstructure under biaxial strains were calculated by applying constrained strains with specific ratios $x\% = (a - a_0)/a_0 \times 100\%$, where a and a_0 are the lattice parameters of the strained and unstrained structures, respectively. The unstrained optimized unit cell was enlarged or compressed symmetrically through different strain values. We have also verified the electronic properties of designed structures under twist to examine the nature of band gap.

III. RESULTS AND DISCUSSION

A. Structural and vibrational properties

Our calculations began with stable AA' stacking (chalcogen atoms of one layer overlap with the metal atoms of another layer and vice versa) in the heterobilayers in order to relax their geometries [41, 42]. The ground state of studied heterobilayers is obtained by minimizing forces on both lattice and atomic positions. The resultant vdW-corrected lattice parameters and interlayer

distances are listed in Table I, which are averaged values of experimental bulk parameters. We have observed that these TMD-based heterobilayers (as illustrated in Fig. 1) have inversion symmetry breaking and belong to $P3m1$ space group with C_{3v} symmetry, which is different from homobilayers having inversion D_{3d} symmetry with $P\bar{6}m2$ space group. This kind of symmetry breaking leads to novel and exceptional features for example in moiré structures [43].

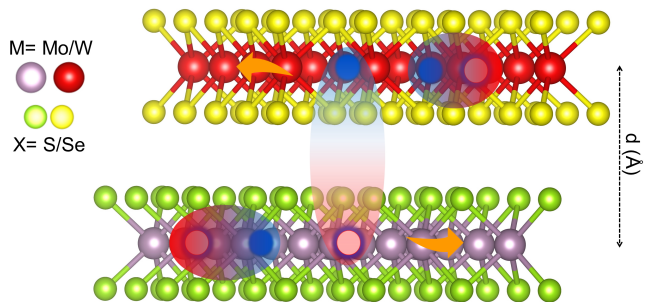


FIG. 1. Schematic representation of a S/Se-based TMD heterobilayer with intralayer and interlayer exciton representations. Excitons in heterobilayers composed of two monolayers are intralayer, comprising electrons and holes in the same monolayer, and interlayer, comprising electrons and holes in subsequent monolayers.

For a better understanding of interlayer interactions, we have calculated their vibrational properties at the Γ -point. The interlayer interactions influence the atomic environment and create attractive or repulsive dipole forces that in turn affect the vibrational modes. A TMD-based heterobilayer has two units of X–M–X layers with C_{3v} symmetry, implying that there are 18 phonon modes, out of which 3 are acoustic ($2E \oplus 1A_1$) and 15 optical ($10E \oplus 5A_1$) involving both in-plane (E) and out-of-plane (A_1) vibrations. All these modes are both Raman and IR active. The Raman spectra of heterobilayers and their monolayers are presented in Fig. 2(a, c), and distinct fingerprints of different vibrational modes of same and different chalcogen-based heterobilayers are depicted in Fig. 2(b, d). The modes in between $150\text{--}250\text{ cm}^{-1}$ & $390\text{--}400\text{ cm}^{-1}$ are from chalcogen atoms, and other modes are due to the metal with chalcogen atoms. We have summarized all the frequency modes and displacements for the studied heterobilayers in Table I. The Raman intensities are magnified approximately twice for the heterobilayers over individual monolayers, which clearly indicates interlayer interactions. The modes above $\sim 150\text{ cm}^{-1}$ correspond to intralayer vibrations of each monolayer present in the heterobilayers. Importantly, we have observed two low-intensity modes below 50 cm^{-1} region, these are due to lateral and vertical dipole-dipole interactions between the two layers in the heterobilayers [44–47]. These low-frequency shear and layer-breathing modes (LBM) have low intensity due to 0K calculations and can be intensified by raising the temperature.

TABLE I. Optimized lattice parameters (in Å) (a), Interlayer distance (in Å) (d), vibrational frequencies (ω , in cm^{-1}) of $\text{MoS}_2/\text{MoSe}_2$, $\text{MoS}_2/\text{WSe}_2$, $\text{WS}_2/\text{MoSe}_2$, WS_2/WSe_2 , MoS_2/WS_2 , and $\text{MoSe}_2/\text{WSe}_2$. All the vibrational frequencies are both IR and Raman active. The experimental values are taken from [48–53]

Structure	a	d	ω (present)	ω (exp.)	Mode
$\text{MoS}_2/\text{MoSe}_2$	3.221	6.333	17.7, 26.7	~ 250	$E(\text{Shear}), A_1(\text{LBM})$
			166.3, 237.8		$E, A_1(\text{Se atom})$
			272.8		$E(\text{S atom})$
			284.9, 350.2		$E, A_1(\text{MoSe}_2 \text{ unit})$
			365.3		$E(\text{MoS}_2 \text{ unit})$
			393.4		$A_1(\text{S atom})$
449.7	$A_1(\text{MoS}_2 \text{ unit})$				
$\text{MoS}_2/\text{WSe}_2$	3.228	6.348	18.4, 25.4	~ 250	$E(\text{Shear}), A_1(\text{LBM})$
			169.3, 240.5		$E, A_1(\text{Se atom})$
			241.2		$E(\text{WSe}_2 \text{ unit})$
			272.1		$E(\text{S atom})$
			301.5		$A_1(\text{WSe}_2 \text{ unit})$
			364.2		$E(\text{MoS}_2 \text{ unit})$
393.2	$A_1(\text{S atom})$				
448.8	$A_1(\text{MoS}_2 \text{ unit})$				
$\text{WS}_2/\text{MoSe}_2$	3.225	6.364	18.5, 22.8	~ 250	$E(\text{Shear}), A_1(\text{LBM})$
			166.2, 237.8		$E, A_1(\text{Se atom})$
			279		$E(\text{S atom})$
			284.8,		$E(\text{MoSe}_2 \text{ unit})$
			333.7		$E(\text{WS}_2 \text{ unit})$
			350.1		$A_1(\text{MoSe}_2 \text{ unit})$
397.2	$A_1(\text{S atom})$				
412.8	$A_1(\text{WS}_2 \text{ unit})$				
WS_2/WSe_2	3.232	6.379	16.5, 20.3	~ 250	$E(\text{Shear}), A_1(\text{LBM})$
			169.3, 240.6		$E, A_1(\text{Se atom})$
			241.1		$E(\text{WSe}_2 \text{ unit})$
			279.2		$E(\text{S atom})$
			301.3		$A_1(\text{WSe}_2 \text{ unit})$
			332.7		$E(\text{WS}_2 \text{ unit})$
397.0	$A_1(\text{S atom})$				
411.8	$A_1(\text{WS}_2 \text{ unit})$				
MoS_2/WS_2	3.162	6.177	19.3, 26.1	~ 31	$E(\text{Shear}), A_1(\text{LBM})$
			278.5, 285.4	$\sim 350, \sim 375$	$E(\text{S atom of both MoS}_2, \text{WS}_2 \text{ units})$
			342.5, 375.5		$E(\text{WS}_2 \text{ unit, MoS}_2 \text{ unit})$
			396.6, 400.5		$A_1(\text{S atom of both MoS}_2, \text{WS}_2 \text{ units})$
			422.8, 459.3		$A_1(\text{WS}_2 \text{ unit, MoS}_2 \text{ unit})$
$\text{MoSe}_2/\text{WSe}_2$	3.296	6.534	16.6, 22.1	~ 237	$E(\text{Shear}), A_1(\text{LBM})$
			164.1, 167.7		$E(\text{Se atom of both MoSe}_2, \text{WSe}_2 \text{ units})$
			236.4		$A_1(\text{Se atom of MoSe}_2 \text{ unit})$
			237.6		$E(\text{WSe}_2 \text{ unit})$
			239.1		$A_1(\text{Se atom of WSe}_2 \text{ unit})$
			279.6		$E(\text{MoSe}_2 \text{ unit})$
296.2, 344.7	$A_1(\text{WSe}_2 \text{ unit, MoSe}_2 \text{ unit})$				

B. Electronic properties

The exact band gap calculation is of primary importance for optoelectronic device performance. It is known that the standard DFT (LDA/GGA) approaches underestimate the electronic band gap owing

to the lack of derivative discontinuity in their exchange-correlation functional associated with the many-body electron-electron interactions. We have accounted for these effects using the G_0W_0 approximation, which provides accurate electronic properties for a wide range of materials [54, 55]. The computed electronic bandstruc-

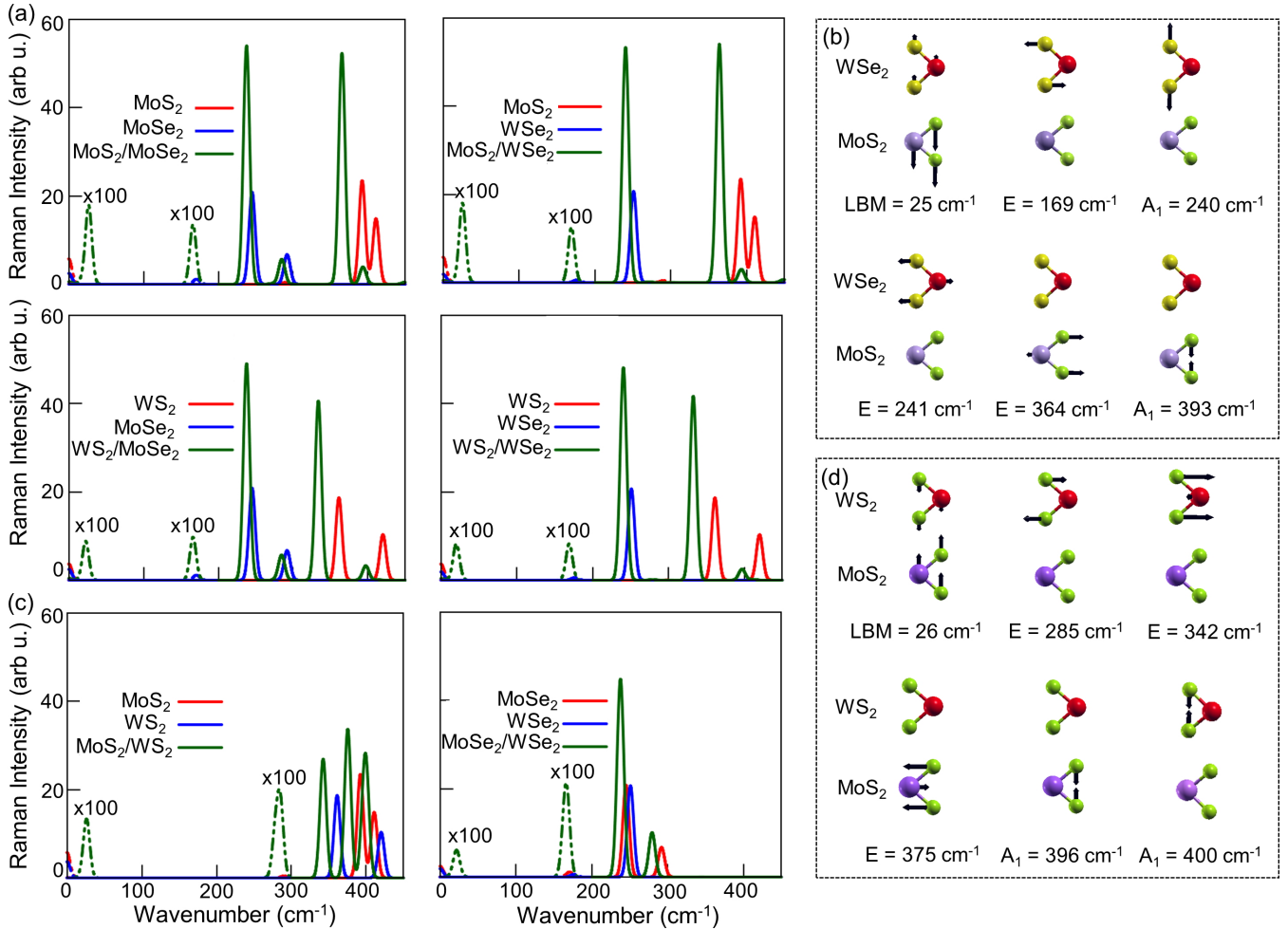


FIG. 2. (a) Computed Raman spectra for MoS₂/MoSe₂, MoS₂/WSe₂, WS₂/MoSe₂ and WS₂/WSe₂ heterobilayers, (b) Illustration of the vibrational modes of MoS₂/WSe₂ heterobilayer. (c) Computed Raman spectra for MoS₂/WS₂ and MoSe₂/WSe₂ heterobilayers, (d) Illustration of the vibrational modes of MoS₂/WS₂ heterobilayer. From this, we can see the displacement of both layers in LBM modes.

ture along with the orbital projected density of states (DOS) for different chalcogen-based heterobilayers are shown in Fig. 3(a), and they show a direct band gap behavior along K-K high symmetry direction dissimilar to the indirect nature of the same chalcogen atom based heterobilayer (MoS₂/WS₂ & MoSe₂/WSe₂) as shown in Fig. 3(b). The band profiles of same chalcogen-based materials are consistent with previous reports, with a slight difference in the band gap values due to the absence of the spin-orbit coupling, which is responsible for lifting the degeneracy in the conduction and valence bands [13, 56]. Direct/indirect band gap in a material depends upon the orbitals involved at the band edges. For different chalcogen-based materials, the transition metal d_{xy} orbitals have major contributions at both band edges and result in a direct band gap. For same chalcogen-based materials, chalcogens p_z orbitals are more dominant at the valence band edge, and the transition metal d_{xy} orbitals populate the conduction band edge, which in turn

changes the gap from direct to indirect. These results suggest that the material will have a direct band gap if $X_1 \neq X_2$ otherwise indirect band gap, as illustrated in Fig. 3(c).

Apart from the nature of the band gap, the band alignment (straddling/staggered/broken) of heterobilayers depends on the band offset of the individual monolayers. We observed type-II band (staggered) alignment with band gap values in the range of 1.4 to 2.0 eV for the heterobilayers considered. The band gap value of MoS₂/WSe₂ is consistent with the reported experimental results [57] while the other heterobilayers require experimental verification. The obtained band gap values of heterobilayers are generally lower than those of TMD monolayers [58] and lie in the near IR region, which makes them useful for infrared applications. In the projected DOS, the valence band maxima is mainly coming from one layer (Se-based monolayer) and the conduction band minima from the other layer (S-based monolayer), as represented

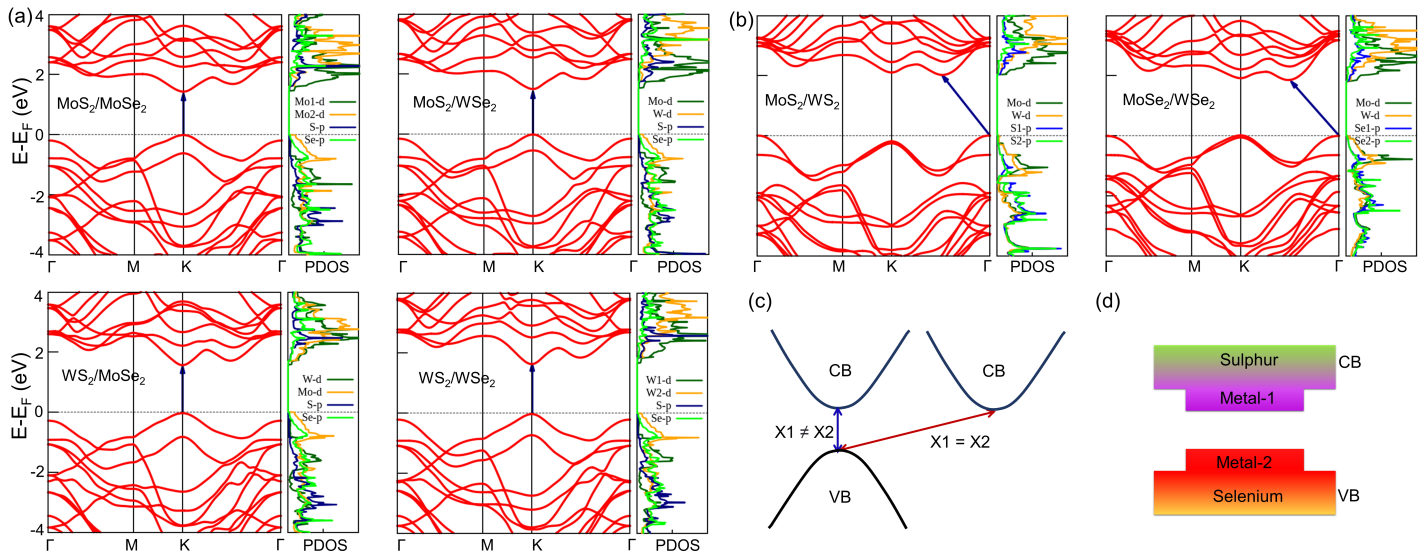


FIG. 3. (a) Electronic bandstructure and projected DOS of different S/Se based heterobilayers using LDA + G_0W_0 approximation. All the compounds show direct band gaps. (b). Electronic bandstructure and projected density of states of same S/Se based heterobilayers using LDA + G_0W_0 approximation. (c) Illustrative representation of direct and indirect band gap behavior based on the chalcogen atoms in MX_2 ($M = \text{Mo/W}$, $X = \text{S/Se}$) based heterobilayers. (d) Illustrative representation of the staggered band alignment of these heterobilayers.

in Fig. 3(d). At the band edges, the metal d -orbitals and chalcogen p -orbitals of each monolayer are highly dominating and the valence band maximum (conduction band minimum) has hybridization between metal- d orbital and Se (S)- p orbital resulting from the covalent bonds within each layer.

C. Optical properties

Excitons of the same chalcogen TMD heterobilayers are well studied but the different chalcogen materials remain unexplored. Our current electronic studies show that different chalcogen heterobilayers have direct band gap and the study of excitons in these materials help to understand the underlying features that control photoluminescence yield and the radiative recombination rate of electrons and holes. These layer-separated electron-hole interactions are examined through the BSE approximation [40] to estimate the optical absorption of hetero-bilayers (shown in Fig. 4) along with the oscillator strengths. The optical band gaps are found in the range of 1.225 to 1.428 eV for heterobilayers, (as shown in Table II), which are interlayer exciton transitions having binding energies in the range of 240-250 meV with weak oscillator strengths due to weak dipole-dipole interactions between the layers. These interlayer excitons are quite stable from thermal dissociation and useful for developing stable optoelectronic devices [59]. It is well known that monolayers show A and B intralayer excitons in the visible spectral region [60–62] with large binding energies, whereas the formation of excitons in different

chalcogen-based heterobilayers lies in infrared spectral domain.

The excitons can be tuned by selecting different metal atoms and by controlling the interlayer interactions. For instance, $\text{MoS}_2/\text{MoSe}_2$ has the lowest electronic band gap, the A and B exciton peaks are located at 1.850 (A_1), 1.997 (A_2), and 2.029 (B_1), 2.057 (B_2) eV, respectively, as shown in Table II. When one of the metal atoms is replaced with W ($\text{MoS}_2/\text{WSe}_2$), the electronic band gap increases, and the peaks corresponding to A and B excitons shift to 1.820 (A_1), 1.831 (A_2) and 2.122 (B_1), 2.212 (B_2) eV, respectively. These two sets of values correspond to the individual monolayers. By replacing the W atoms with Mo, we can maximize the band gaps in the studied heterobilayers and cause a slight shift in the A, and B exciton peaks. The localization of e^- and hole pairs within the layer has high oscillator strengths, and their delocalization reduces oscillator strengths which are observed for interlayer excitons. The energetic positions of exciton peaks are slightly shifted compared to individual monolayers because of small dielectric screening along the out of plane direction. The current result closely matches with the reported experimental photoluminescence measurements of the heterobilayers [12, 16, 48, 63].

D. Band gap nature under strain and twist

In the previous sections, we evaluated the electronic and optical properties of structurally relaxed heterobilayers, where the lattice constant is average of both individual monolayers. The change in lattice parameter

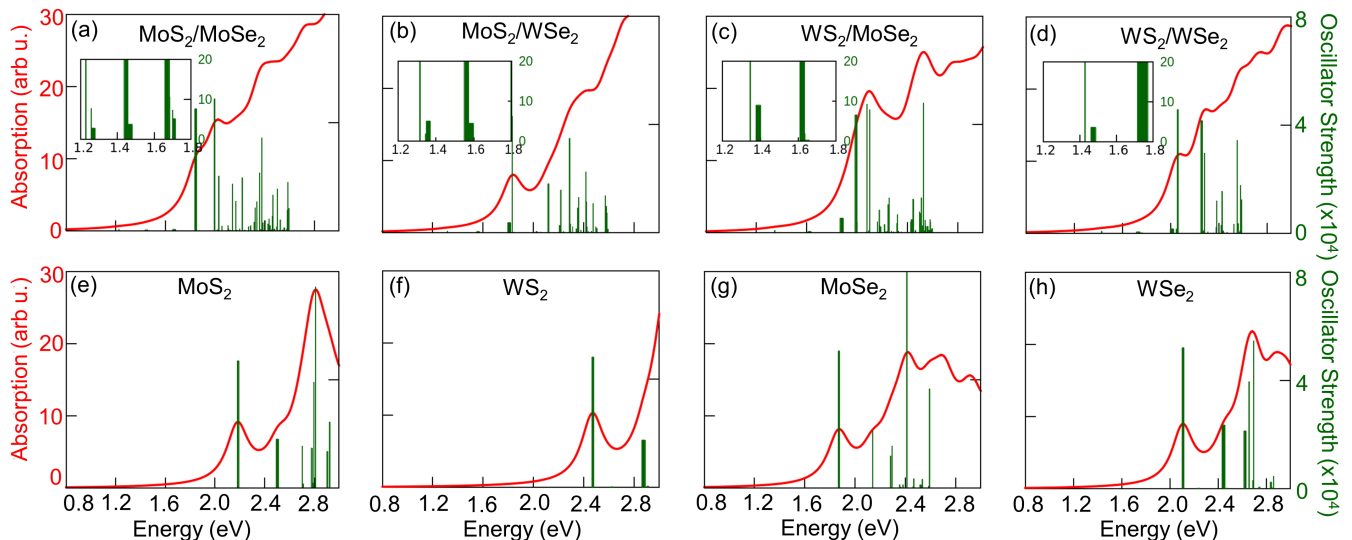


FIG. 4. Optical absorption spectra for (a) MoS₂/MoSe₂, (b) MoS₂/WSe₂, (c) WS₂/MoSe₂ and (d) WS₂/WSe₂ heterobilayer and independent monolayers (e) MoS₂, (f) MoSe₂, (g) WS₂ and (h) WSe₂ along with the oscillator strength. The insets illustrate the oscillator strength around the lowest interlayer excitonic peaks.

Material	E_g (LDA)	E_g (G_0W_0)	E_g (Optical)	A exciton	B exciton	Binding energy
MoS ₂ /MoSe ₂	0.861	1.465	1.225	A ₁ -1.850, A ₂ -1.997	B ₁ -2.029, B ₂ -2.057	0.240
MoS ₂ /WSe ₂	0.654	1.560	1.315	A ₁ -1.820, A ₂ -1.831	B ₁ -2.122, B ₂ -2.212	0.245
WS ₂ /MoSe ₂	1.117	1.591	1.345	A ₁ -1.889, A ₂ -1.991	B ₁ -2.078, B ₂ -2.100	0.246
WS ₂ /WSe ₂	0.946	1.679	1.428	A ₁ -2.049, A ₂ -2.055	B ₁ -2.262, B ₂ -2.280	0.251

TABLE II. Obtained band gaps using LDA, G_0W_0 approximations, Optical band gap, intralayer A and B exciton positions and exciton binding energies of the studied heterobilayers. All energies are in eV.

affects the fundamental properties as observed in earlier report on MoSe₂/MoS₂, shows the band gap behavior changing from direct to indirect [63]. This distinct behavior indicates an external strain acting on these materials plays a vital role in describing their electronic properties. In this aspect, we explore the electronic band gap behavior by applying mechanically constricted strain to the relaxed geometries. Here, the strain is applied in-plane, out-of-plane and both together. As shown in Fig. 5, a minimal strain changes the band gap and its nature along the momentum direction. By applying in-plane compression, we observed the smooth change in the band gap from direct to indirect, and for the out-of-plane compressions, the band gap changes occurred asymptotically. The out-of-plane strain (vdW interactions) influence the band gap nature between 2-4% applied strain in MoS₂/WSe₂, WS₂/WSe₂ and below 1% external strain for MoS₂/MoSe₂. But WS₂/MoSe₂ doesn't change the band gap nature within 4% of strain. Whereas, the simultaneous in and out-of-plane compression changes the

band gap nature within 2% of the compression strain, effectively due to the dominance of in-plane interactions. These results opens the door to tune the band gap and its nature from direct to indirect and vice versa by selective strain in TMD heterobilayers through experiments.

In addition, the lattice mismatch in the individual layers plays a crucial role in forming the commensurate structures for the TMD heterobilayers. For instance, the same chalcogen-based monolayers ($M_1 \neq M_1$, $X_1 = X_2$) possess a lattice mismatch of 0.3%, and different chalcogen-based layers ($X_1 \neq X_2$) have a lattice mismatch of 3.8%. Recent report on MoS₂/WSe₂ commensurate structure with a 16° twist angle exhibited both direct and indirect band gap behavior [16], flagged the importance of twist in TMD heterobilayers. Hence, we examined the 16° twist angle heterobilayers in the present work, and these twisted supercells are generated by simulating the structure with the twister code [64]. The new supercell lattice vectors (called X and Y) are related to the lattice

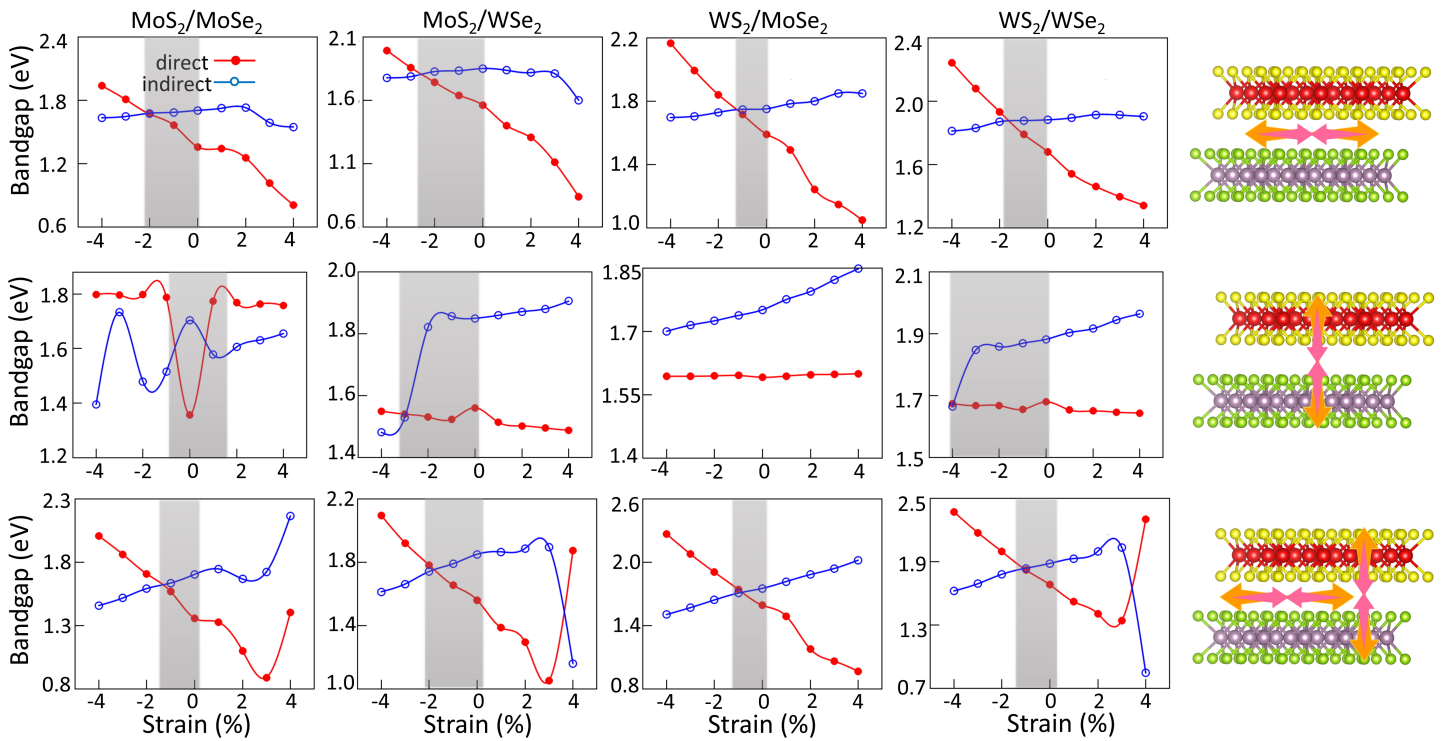


FIG. 5. Effect of different constrained strains to examine the nature of the band gap behavior for TMD-based heterobilayers using LDA + G_0W_0 approximation, *Top panel*: In-plane strain with a fixed interlayer distance, *Middle panel*: Out of plane strain at a fixed in-plane lattice constant, *Bottom panel*: Biaxial strain, where both in- and out-of-plane parameters are varied

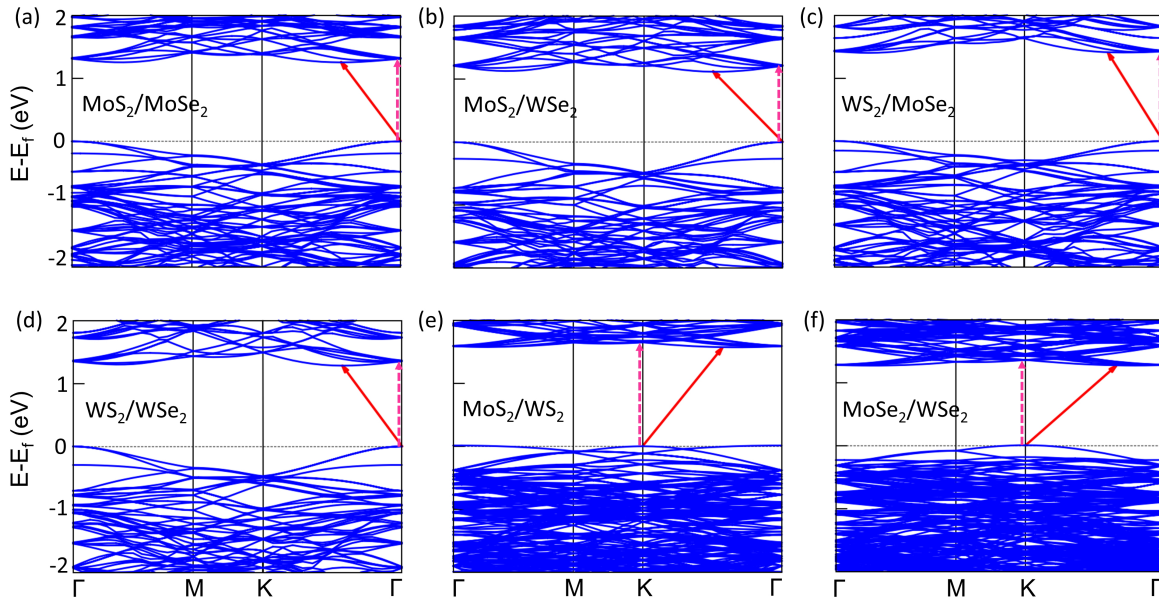


FIG. 6. Calculated folded bandstructure for 16° twisted heterobilayers using LDA approximation for (a) $\text{MoS}_2/\text{MoSe}_2$, (b) $\text{MoS}_2/\text{WSe}_2$, (c) $\text{WS}_2/\text{MoSe}_2$, (d) WS_2/WSe_2 , (e) MoS_2/WS_2 , and (f) $\text{MoSe}_2/\text{WSe}_2$ (red line indicates indirect band gap and pink line represents direct band gap)

vectors of each monolayer through the following matrices:

$$\begin{bmatrix} X \\ Y \end{bmatrix} = T \begin{bmatrix} x_1(M_1X_1) \\ y_1(M_1X_1) \end{bmatrix} = T' \begin{bmatrix} x_2(M_2X_2) \\ y_2(M_2X_2) \end{bmatrix} \quad (1)$$

where $x_1(M_1X_1)$, $y_1(M_1X_1)$, $x_2(M_2X_2)$ and $y_2(M_2X_2)$ are the lattice vectors of each monolayer respectively, T

and T' are transformation matrices given by

$$T = \begin{pmatrix} 3 & -4 \\ 4 & -1 \end{pmatrix} \text{ and } T' = \begin{pmatrix} 2 & -4 \\ 4 & -2 \end{pmatrix} \quad (2)$$

The supercell generated with these vectors contains a larger number of atoms, and dealing with such large structures using G_0W_0 methodology is computationally expensive. Thus, we calculated these band structures using the LDA approximation with $8 \times 8 \times 1$ k-point mesh. The resultant folded electronic band structures are shown in Fig. 6. It is clearly evident that different (same) chalcogen-based heterobilayers shows the momentum-indirect band gap in between $\Gamma - K$ ($K - \Gamma$) and an energy difference of 10-100 meV with the momentum-direct band gap nature along the $\Gamma(K)$ - high symmetry direction (band values are given in Table III). Interestingly, we found that the bandwidth of valence and conduction bands are decreased from untwisted to twisted heterobilayers, suggesting the possibility of obtaining flat-bands with twist angle. These findings of TMD-heterobilayers have shown great possibilities to tune the electronic and optical properties with minimal twist and strain for optoelectronics and solar-cell device applications.

IV. CONCLUSIONS

In summary, we have explored the electronic and optical properties of MX_2 ($M = \text{Mo/W}$, $X = \text{S/Se}$) heterobilayers using first-principles density functional theory calculations. Designed heterobilayers of TMD-based materials exhibited inversion symmetry breaking with point group C_{3v} , shows Raman fingerprints of individual monolayers are at higher frequencies ($> 150 \text{ cm}^{-1}$) and below 50 cm^{-1} correspond to the shear or layer breathing modes due to the atomic environment & interlayer interactions. We have used the G_0W_0

method to calculate accurate electronic properties and found that the electronic band gaps are in the range of 1.4 to 2.0 eV with staggered band alignment. We found that the band gap behavior changes from direct to indirect and vice versa by choice of the chalcogen (same/different) atoms in the heterobilayers. The absorption spectra are calculated using BSE methodology and obtained the exciton binding energies for different chalcogen-based heterobilayers are in the order of 250 meV due to strong interlayer interactions. We also investigated the electronic bandstructures under the in-plane, out-of-plane strains & twist angle between heterobilayers and observed change in band gap nature and its values. Our results demonstrate that, under minimal strain, different chalcogen-based heterobilayers can change their band gap from direct to indirect owing to their interlayer interactions. These outcomes of TMD-heterobilayers have shown great possibilities to tailor the electronic and optical properties with minimal twist for tunable optoelectronic applications.

ACKNOWLEDGMENTS

RB would like to thank UGC for the senior research fellowship and computational facilities at IITJ. This work is funded by Science and Engineering Research Board (SERB) grant number R/JF/2021/000147 (SA), SERB:CRG/2022/008749 (BMKM), IITJ seed grant:I/SEED/BMK/20230017 (BMKM) and the Korean NRF through Grants with No. 2020R1A2C3009142 (N.L.). We are grateful to the computational facilities from KISTI Grant No. KSC-2022-CRE-0514 and the resources of Urban Big data and AI Institute (UBAI). J.J. acknowledges the Korean NRF grant with No. 2020R1A5A1016518 and the Korean Ministry of Land, Infrastructure and Transport (MOLIT) from the Innovative Talent Education Program for Smart Cities.

-
- [1] J. R. Schaibley, H. Yu, G. Clark, P. Rivera, and J. S. Ross, *Nat. Rev. Mater.* **1**, 16055 (2016).
 - [2] Y. Ominato, J. Fujimoto, and M. Matsuo, *Phys. Rev. Lett.* **124**, 166803 (2020).
 - [3] H. M. Hill, A. F. Rigosi, C. Roquelet, A. Chernikov, T. C. Berkelbach, D. R. Reichman, M. S. Hybertsen, L. E. Brus, and Tony F. Heinz, *Nano Lett.* **15**, 2992 (2015).
 - [4] C. Alexey, B. C. Timothy, H. M. Hill, A. Rigosi, L. Yilei, B. Aslan, D. R. Reichman, M. S. Hybertsen, and T. F. Heinz, *Phys. Rev. Lett.* **113**, 076802 (2014).
 - [5] M. M. Ugeda, A. J. Bradley, S. F. Shi, F. H. Da Jornada, Y. Zhang, D. Y. Qiu, W. Ruan, S. K. Mo, Z. Hussain, Z. X. Shen, F. Wang, S. G. Louie, and M. F. Crommie, *Nat. Mater.* **13**, 1091 (2014).
 - [6] T. Mueller and E. Malic, *npj 2D Mater. Appl.* **2**, 29 (2018).
 - [7] A. Pospischil and Thomas Mueller, *Appl. Sci.* **6**, 78 (2016).
 - [8] Q. Zeng and Z. Liu, *Adv. Electron. Mater.* **4**, 1700335 (2018).
 - [9] J. Cheng, C. Wang, X. Zou, and L. Liao, *Adv. Opt. Mater.* **7**, 1800441 (2018).
 - [10] Y. Liu, N. O. Weiss, X. Duan, H. C. Cheng, Y. Huang, and X. Duan, *Nat. Rev. Mater.* **1**, 16042 (2016).
 - [11] X. Zhou, X. Hu, J. Yu, S. Liu, Z. Shu, Q. Zhang, H. Li, Y. Ma, H. Xu, and T. Zhai, *Adv. Funct. Mater.* **28**, 1706587 (2018).
 - [12] D. Kozawa, A. Carvalho, I. Verzhbitskiy, F. Giustiniano, Y. Miyauchi, S. Mouri, A. H. Castro Neto, K. Matsuda, and G. Eda, *Nano Lett.* **16**, 4087 (2016).
 - [13] E. Torun, P. C. Henrique Miranda, A. Molina-Sánchez, and L. Wirtz, *Phys. Rev. B* **97**, 245427 (2018).
 - [14] Y. Jiang, S. Chen, W. Zheng, B. Zheng, and A. Pan, *Light Sci. Appl.* **10**, 72 (2021).
 - [15] E. V. Calman, M. M. Fogler, L. V. Butov, S. Hu, A. Mishchenko and A. K. Geim, *Nat. Commun.* **9**, 1895

Material	Without twisted geometry		With twisted geometry		Twisted geometry $\Delta E_{(direct - indirect)}$ (meV)	Without twisted geometry $\Delta E_{(direct - indirect)}$ (meV)
	VB (eV)	CB (eV)	VB (eV)	CB (eV)		
MoS ₂ /MoSe ₂	0.853	0.978	0.432	0.155	57	255
MoS ₂ /WSe ₂	0.866	0.999	0.619	0.155	92	336
WS ₂ /MoSe ₂	0.833	1.037	0.497	0.225	18	150
WS ₂ /WSe ₂	0.877	1.058	0.614	0.210	68	217
MoS ₂ /WS ₂	1.340	0.963	0.167	0.078	78	61
MoSe ₂ /WSe ₂	1.111	1.325	0.348	0.088	85	82

TABLE III. Calculated linewidth of the valence and conduction bands without and with twist geometry. Direct to indirect band gap difference in twisted and relaxed structures

- (2018).
- [16] O. Karni, E. Barré, S. C. Lau, R. Gillen, E. Y. Ma, B. Kim, K. Watanabe, T. Taniguchi, J. Maultzsch, K. Barkmak, R. H. Page, and T. F. Heinz, *Phys. Rev. Lett.* **123**, 247402 (2019).
- [17] B. Miller, A. Steinhoff, B. Pano, J. Klein, F. Jahnke, A. Holleitner, and U. Wurstbauer, *Nano Lett.* **17**, 5229 (2017).
- [18] C. Jiang, W. Xu, A. Rasmita, Z. Huang, K. Li, Q. Xiong, and W. Gao, *Nat. Commun.* **9**, 753 (2018).
- [19] L. A. Jauregui, A. Y. Joe, K. Pistunova, D. S. Wild, A. A. High, Y. Zhou, G. Scuri, K. D. Greve, A. Sushko, C. H. Yu, T. Taniguchi, K. Watanabe, D. J. Needleman, M. D. Lukin, H. Park, and P. Kim, *Science* **366**, 870 (2019).
- [20] Y. Liu, H. Fang, A. Rasmita, Y. Zhou, J. Li, T. Yu, Q. Xiong, N. Zheludev, J. Liu, and W. Gao, *Sci. Adv.* **5**, (2019).
- [21] H. J. Liu, L. Jiao, L. Xie, F. Yang, J. L. Chen, W. K. Ho, C. L. Gao, J. F. Jia, X. D. Cui, and M. H. Xie, *2D Mater.* **2**, 034004 (2015).
- [22] S. Jo, N. Ubrig, H. Berger, A. B. Kuzmenko, and A. F. Morpurgo, *Nano Lett.* **14**, 2019 (2014).
- [23] I. C. Gerber, E. Courtade, S. Shree, C. Robert, T. Taniguchi, K. Watanabe, A. Balocchi, P. Renucci, D. Lagarde, X. Marie, and B. Urbaszek, *Phys. Rev. B* **99**, 035443 (2019).
- [24] R. Gillen and J. Maultzsch, *Phys. Rev. B* **97**, 165306 (2018).
- [25] J. Madéo, M. K. L. Man, C. Sahoo, M. Campbell, V. Pareek, E. Laine Wong, A. Al-Mahboob, N. S. Chan, A. Karmakar, B. M. K. Mariserla, X. Li, T. F. Heinz, T. Cao, and K. M. Dani, *Science* **370**, 1199 (2020).
- [26] C. Robert, B. Han, P. Kapuscinski, A. Delhomme, C. Faugeras, T. Amand, M. R. Molas, M. Bartos, K. Watanabe, T. Taniguchi, B. Urbaszek, M. Potemski, and X. Marie, *Nat. Commun.* **11**, 4037 (2020).
- [27] M. R. Molas, C. Faugeras, A. O. Slobodeniuk, K. Nogajewski, M. Bartos, D. M. Basko, and M. Potemski, *2D Mater.* **4**, 021003 (2017).
- [28] Z. Khatibi, M. Feierabend, M. Selig, S. Brem, C. Linderälv, P. Erhart, and E. Malic, *2D Mater.* **6**, 015015 (2019).
- [29] S. Gao, L. Yang, and C. D. Spataru, *Nano Lett.* **17**, 7809 (2017).
- [30] L. Liang and V. Meunie, *Nanoscale* **6**, 5394 (2014).
- [31] H. Sahin, S. Tongay, S. Horzum, W. Fan, J. Zhou, J. Li, J. Wu, and F. M. Peeters, *Phys. Rev. B* **87**, 165409 (2013).
- [32] B. Amin, T. P. Kaloni, G. Schreckenbach, and M. S. Freund, *Appl. Phys. Lett.* **108**, 063105(2016).
- [33] J. Kang, S. Tongay, and J. Zhou, *Appl. Phys. Lett.* **102**, 012111 (2013).
- [34] Q. Li, L. Tang, C. Zhang, D. Wang, Q. Chen, Y. Feng, L. Tang, and K. Chen, *Appl. Phys. Lett.* **111**, 171602 (2017).
- [35] P. Giannozzi, O. Baseggio, P. Bonfà, D. Brunato, R. Car, I. Carnimeo, C. Cavazzoni, S. Gironcoli, P. Delugas, F. F. Ruffino, A. Ferretti, N. Marzari, I. Timrov, A. Urru, and S. Baroni, *J. Chem. Phys.* **152**, 154105 (2020).
- [36] J.P. Perdew and A. Zunger, *Phys. Rev. B* **23**, 5048 (1981).
- [37] J. Klimes, D. R. Bowler, and A. Michaelides, *Phys. Rev. B* **83**, 195131 (2011).
- [38] A. D. Corso, S. Baroni, and R. Resta, *Phys. Rev. B* **47**, 3588 (1993).
- [39] L. Hedin, *Phys. Rev.* **139**, A796 (1965).
- [40] X. Leng, F. Jin, M. Wei, and Y. Ma, *WIREs Comput. Mol. Sci.* **6**, 532 (2016).
- [41] J. He, K. Hummer, and C. Franchini, *Phys. Rev. B* **89**, 075409 (2014).
- [42] W. Li, T. Wang, X. Dai, X. Wang, C. Zhai, Y. Ma, S. Chang, *Solid State Commun.* **225**, 32 (2016).
- [43] J. Jung, A. M. DaSilva, A. H. MacDonald, and S. Adam, *Nat. Commun.* **20**, 1 (2015).
- [44] P. H. Tan, W. P. Han, W. J. Zhao, Z. H. Wu, K. Chang, H. Wang, Y. F. Wang, N. Bonini, N. Marzari, N. Pugno, G. Savini, A. Lombardo, and A. C. Ferrari, *Nat. Mater.* **11**, 294 (2012).
- [45] Y. Zhao, X. Luo, H. Li, J. Zhang, P. T. Araujo, C. K. Gan, J. Wu, H. Zhang, S. Y. Quek, M. S. Dresselhaus, and Q. Xiong, *Nano Lett.* **13**, 1007 (2013).
- [46] X. Zhang, W. P. Han, J. B. Wu, S. Milana, Y. Lu, Q. Q. Li, A.C. Ferrari, and P. H. Tan, *Phys. Rev. B* **87**, 115413 (2013).

- [47] C. H. Lui, Z. Ye, C. Ji, K. C. Chiu, C. T. Chou, T. I. Andersen, C. M. Shively, H. Anderson, J. M. Wu, T. Kidd, Y. H. Lee, and R. He, *Phys. Rev. B* **91**, 165403 (2015).
- [48] T. Ye, J. Li, and D. Li, *Small* **15**, 1902424 (2019).
- [49] Y. C. Lin, R. K. Ghosh, R. Addou, N. Lu, S. M. Eichfeld, H. Zhu, M. Y. Li, X. Peng, M. J. Kim, L. J. Li, R. M. Wallace, S. Datta, and J. A. Robinson, *Nat. Commun.* **6**, 731 (2015).
- [50] M. S. Kim, C. Seo, H. Kim, J. Lee, D. H. Luong, J. H. Park, G. H. Han, and J. Kim, *ACS Nano* **10**, 6211 (2016).
- [51] J. Zhang, J. Wang, P. Chen, Y. Sun, S. Wu, Z. Jia, X. Lu, H. Yu, W. Chen, J. Zhu, G. Xie, R. Yang, D. Shi, X. Xu, J. Xiang, K. Liu, and G. Zhang, *Adv. Mater.* **28**, 1950 (2016).
- [52] N. Choudhary, J. Park, J. Y. Hwang, H. S. Chung, K. H. Dumas, S. I. Khondaker, W. Choi, and Y. Jung, *Sci. Rep.* **6**, 25456 (2016).
- [53] X. Fu, F. Li, J. F. Lin, Y. Gong, X. Huang, Y. Huang, H. Gao, Q. Zhou, and T. Cui, *J. Phys. Chem. C* **122**, 5820 (2018).
- [54] S. Appalakondaiah, G. Vaitheeswaran, and S. Lebègue, *J. Chem. Phys.* **138**, 184705 (2013).
- [55] S. Appalakondaiah, G. Vaitheeswaran, and S. Lebègue, *J. Phys. Chem. A* **119**, 6574 (2015).
- [56] L. Debbichi, O. Eriksson, and S. Lebègue, *Phys. Rev. B* **89**, 205311 (2014).
- [57] M. H. Chiu, X. M. Li, X. W. Zhang, W. T. Hsu, W. H. Chang, M. Terrones, H. Terrones, and L. J. Li, *ACS Nano* **8**, 9649 (2014).
- [58] H. Kim and H. J. Choi, *Phys. Rev. B* **103**, 085404 (2021).
- [59] S. Lukman, L. Ding, L. Xu, Y. Tao, A. C. Riis-Jensen, G. Zhang, Q. Y. Steve Wu, M. Yang, S. Luo, C. Hsu, L. Yao, G. Liang, H. Lin, Y. W. Zhang, K. S. Thygesen, Q. J. Wang, and Y. F. Jinghua Teng, *Nat. Nanotechnol.* **15**, 675 (2020).
- [60] M. Palumbo, M. Bernardi, and J. C. Grossman, *Nano Lett.* **15**, 2794 (2015).
- [61] F. Ceballos, Q. Cui, M. Z. Bellus, and H. Zhao, *Nanoscale* **8**, 11681 (2016).
- [62] B. Zhu, X. Chen, and X. Cui, *Sci. Rep.* **5**, 9218 (2015).
- [63] A. Arora, P. K. Nayak, S. Bhattacharyya, N. Maity, A. K. Singh, A. Krishnan, and M. S. Ramachandra Rao, *Phys. Rev. B* **103**, 205406 (2021).
- [64] M. H. Naik and M. Jain, *Phys. Rev. Lett.* **121**, 266401 (2018).